Accurate analytical expression of the electrostatic potential close to a grid placed between two plates

G Orjubin

F´SATI, Cape Peninsula University of Technology, Bellville 7535, South Africa

Email: orjubing@cput.ac.za

Abstract. The potential distribution between a grid and two plates is an electrostatic problem already solved for MultiWire detectors used in Nuclear Physics, where theoretical expressions are obtained assuming linear charge distributions. In this paper, the accuracy of the line model is investigated close to the wires, using both analytical and numerical approaches. In the symmetric case where the grid is at equal distances between two grounded plates, it is shown that the error can be modeled using a quadrupole charge. After solving the electrostatic problem for the asymmetric case, a larger discrepancy is found, and is interpreted as a consequence of a dipole charge on the electrode. Two different models of this dipole are then implemented, leading to an accurate theoretical expression of the potential.

1. Introduction

The potential distribution created by a conductive grid is a classical electrostatic problem solved several decades ago [1]. In engineering, its solution is used to model systems containing a grid, *e.g.* electrostatic precipitators [2]. Another application is the MultiWire Proportional Counter (MWPC) invented in the ‘70s for Nuclear Physics [3]. This case has been intensively investigated, the analytical expression of the potential distribution being derived from a line model of the electrodes [4], thus considering wires as lines instead of cylinders.

The validity of this assumption is discussed in this paper. As a reference for precise determination, Laplace’s equation is solved numerically using Comsol Multiphysics®, a commercial Finite Element Model (FEM) package.

Recent literature on this topic puts a focus on the numerical approach [5], particularly useful when space charge effects are considered [6]. However, accurate analytical expressions are always necessary to design a prototype containing conductive grids, justifying the investigation presented herein. Moreover, while expressions given in [4] only apply when the grid is placed between two grounded plates, our results are readily usable for an arbitrary configuration.

The paper is organized as follows: in section 3, a classical formula of the symmetric case (*i.e.* grid at equal distance between grounded plates) is recalled, and a first study of the potential on the conductor surface is done using both theoretical and numerical approaches. Then the general case, or asymmetric, is considered in section 4: after solving the electrostatic problem, it is seen that a dipole behavior of higher strength characterizes the line expression used for MWPC. In order to cope with this small but not negligible error, two models of this dipole are then presented and discussed.

2. Geometry

The geometry under investigation is described in figure 1.

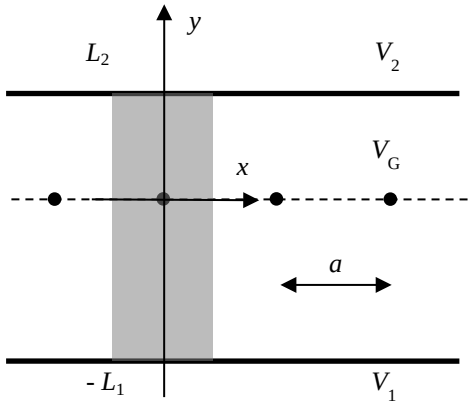

Figure 1. Cross-section of the grid with the two parallel plates.

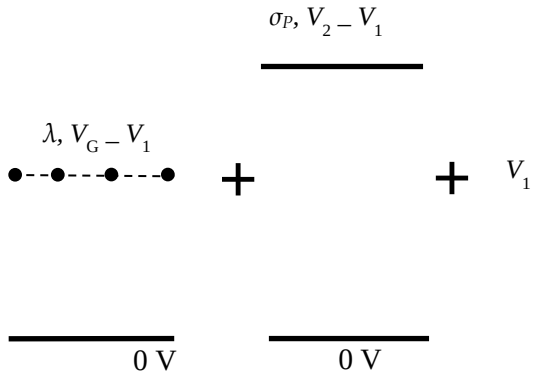

Figure 2. Linear superposition used in the appendix.

Electrodes are situated on the line $y = 0$ at $x = ka$ where *k* is an integer. These wires are cylinders out-of-the plane *x*-*y* with radius r_0. The distance between two parallel wires is *a*. Their charge per unit length, λ, depends on the potentials V_1, V_2 and V_G applied to the conductors.

To solve this 2D electrostatic problem it is convenient to use the complex-valued variable

$$\xi = \pi \frac{z}{a} \tag{1}$$

with $z = x + jy$, as well as the complex electrostatic potential $\Phi(z)$ such as $V(x, y) = \mathrm{Re}[\Phi(z)]$.

Throughout this paper, $a = 1\,\mathrm{mm}$ and $r_0 = 12.5\,\mu\mathrm{m}$.

3. Symmetric case

3.1. General results

In the symmetric case, the grid is located midway between the two grounded plates, thus $L_1 = L_2 = L$ and $V_1 = V_2 = 0$. The expression of the complex potential can be found in [4], where unit linear charge and CGS units were adopted. With a linear charge λ and MKS units, this potential is

$$\Phi_{line} = \frac{L\lambda}{2\varepsilon_0 a} - \frac{\lambda}{2\pi\varepsilon_0} \log\left(2 \frac{\sin\xi - q^2 \sin 3\xi + q^6 \sin 5\xi - \ldots}{1 - 2(q\cos 2\xi - q^4 \cos 4\xi + \ldots)} \right) \tag{2}$$

with $q = \exp\left(\frac{-4\pi L}{a} \right)$.

In our case, $L = 10\,\mathrm{mm}$, so $q = 2.7\times10^{-55}$, a negligible value that leads to the following approximation

$$\Phi_{line} \cong \frac{L\lambda}{2\varepsilon_0 a} - \frac{\lambda}{2\pi\varepsilon_0} \log(2\sin\xi). \tag{3}$$

The potential on the wire surface is $V_{line}(z = r_0\, e^{j\theta})$ and can be expressed using the fact that $r_0 << a$; the first order approximation $\sin\xi \cong \xi$ yields a uniform distribution, *i.e.* V_{line} does not depend on θ. This constant is the potential V_G applied to the conductor:

$$V_G = \frac{L\lambda}{2\varepsilon_0 a} - \frac{\lambda}{2\pi\varepsilon_0}\log\rho \tag{4}$$

with $\rho = \frac{2\pi r_0}{a}$.

3.2. High order approximation on the wire

The third order approximation of $\sin\xi$ in equation (3) actually leads to

$$\Phi_{line} \cong \frac{L\lambda}{2\varepsilon_0 a} - \frac{\lambda}{2\pi\varepsilon_0}\log\rho + \frac{j\theta\lambda}{2\pi\varepsilon_0} + \frac{\lambda}{12\pi\varepsilon_0}\left(\frac{\pi r_0}{a}\right)^2 e^{2j\theta}. \tag{5}$$

The corresponding physical potential on the wire is the real part of this, and can be written as

$$V_{line}(z = r_0 e^{j\theta}) = V_G + V_{0Quad}\cos 2\theta, \tag{6}$$

with $V_{0Quad} = \frac{\lambda}{12\pi\varepsilon_0}\left(\frac{\pi r_0}{a}\right)^2$.

The second term of equation (6) can be interpreted as the contribution of an electric quadrupole [7], and finds its origin in the fact that equipotential lines derived from equation (3) are not exactly circles.

3.3. Numerical validation using FEM

The commercial FEM-based package Comsol Multiphysics ® is used to solve the Laplace´s equation in the shaded domain represented in figure 1. Boundary conditions are V_G = 10 V on the grid, 0 V on the plates, and the zero charge condition $\vec{E}.\vec{n} = 0$ is implemented on the lateral faces. In order to improve the resolution, the finer mesh is selected, and 4th order shape functions are used during discretization. Finally, the numerical problem with 81×10^3 degrees of freedom is solved in 3 s CPU time (dual core I7, 32 Go RAM) using a direct solver. The accuracy of the numerical analysis is 10^{-9}.

The difference between the almost exact numerical FEM solution and the approximate line model is plotted in figure 3.

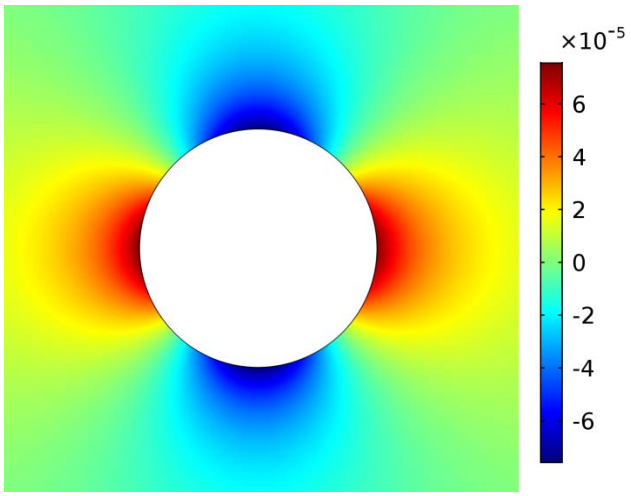

Figure 3. Surface plot of $V_{FEM} - V_{line}$. Close view around the wire for a symmetric case.

This plot illustrates the quadrupole behaviour previously explained in section 3.2. The amplitude $V_{0\,Quad} = 6.5\times10^{-5}\ \mathrm{V}$ of this quadrupole is well predicted by equation (6).

4. Asymmetric case

The asymmetric case, where the grid at potential V_G is not situated midway between two parallel plates at potentials V_1 and V_2, is now presented.

4.1. General equations

As mentioned in [4], equation (3) is the expression for an isolated grid and the constant term enables a matching on the wire. Because the field created by an isolated grid is symmetric, this kind of expansion is not relevant for the asymmetric case. To solve this electrostatic problem, generic methods such as superposition, images and matrix of capacitance can be used [3]. Developments are done in the appendix, leading to the following expression of the complex potential created by this line distribution (placed at $y = 0$) under the influence of the plates

$$\Phi_{line} = V_1 - \frac{\lambda}{2\pi\varepsilon_0}\log\frac{\sin\xi}{\sin\left(\xi + \dfrac{2j\pi L_1}{a}\right)} - j\frac{\sigma_P}{\varepsilon_0}(z + jL_1), \tag{7}$$

where the induced charges λ and σ_P are given in equations (A4-5) as functions of V_G, V_1, and V_2.

4.2. Approximation on the wire

When approximating equation (7) on the wire, one finds that

$$\Phi_{line}(r_0\, e^{j\theta}) \cong V_1 + \frac{\lambda L_1}{\varepsilon_0 a} - \frac{\lambda\log\rho}{2\pi\,\varepsilon_0} + \frac{\sigma_P L_1}{\varepsilon_0} - \frac{\lambda}{2\pi\varepsilon_0}\left(-j\frac{\pi}{2} + j\theta + j\xi - \frac{1}{6}\xi^2\right) - j\frac{\sigma_P r_0\, e^{j\theta}}{\varepsilon_0}. \tag{8}$$

Using the expression of the potential V_G on the grid given in equation (A3), the real potential becomes

$$V_{line}(r_0 e^{j\theta}) \cong V_G + \frac{r_0}{\varepsilon_0}\left(\frac{\lambda}{2a} + \sigma_P\right)\sin\theta + \frac{\lambda}{12\pi\varepsilon_0}\left(\frac{\pi r_0}{a}\right)^2\cos 2\theta. \tag{9}$$

Similar to the symmetric case, the line model presents a quadrupole contribution $V_{quad} = V_{0\,Quad}\cos 2\theta$ with the same amplitude seen in equation (6) for the symmetric case. Moreover, it is interesting to notice that a dipole component

$$V_{dip} = V_{0\,Dip}\sin\theta \tag{10}$$

also exists, with the amplitude $V_{0\,Dip} = \dfrac{r_0}{\varepsilon_0}\left(\dfrac{\lambda}{2a} + \sigma_P\right)$.

It can be noted that for the symmetric case, equations (A4-5) lead to $\sigma_P = -\dfrac{\lambda}{2a}$, meaning that equation (9) reduces to equation (6).

4.3. FEM results

The studied asymmetric configuration is characterized by $L_1 = 10\,\mathrm{mm}$, $L_2 = 5\,\mathrm{mm}$, $V_1 = -5\,\mathrm{V}$, $V_2 = 10\,\mathrm{V}$, and $V_G = 2\,\mathrm{V}$. Figure 4 shows the difference between the field *V* obtained by FEM and the theoretical one associated to a line distribution, *i.e.* equation (7).

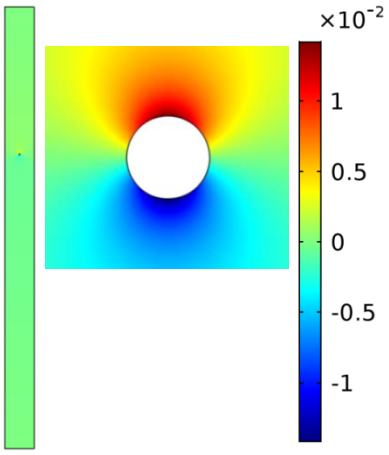

Figure 4. General and close view around the wire of $V_{FEM} - V_{line}$ for an asymmetric case.

Figure 4 exhibits a very small difference between V_{FEM} and V_{line} over the computational domain, except close to the wire where a dipole behaviour is noted. The maximum error is actually equal to $V_{0\,Dip} = 1.4 \times 10^{-2}$ V, which is in agreement with equation (10).

It is noticeable that this error is much larger than the one obtained for the symmetric case. It is therefore of interest to investigate this case and model this dipole behaviour.

4.4. Dipole modelling

It is well-known [1] that a grounded cylindrical conductor placed in an external electric field $\vec{E}_{ext}$ behaves like an electric dipole. In our case $\vec{E}_{ext} = -E_{ext}\,\vec{u}_y$ for $y < 0$. Solving the Laplace's equation for this classical problem gives $V = E_{ext}\left(r - \frac{r_0^2}{r}\right)\sin\theta$: We recognize the external potential $V_{ext} = E_{ext}\, r \sin\theta = E_{ext}\, y$ and an additive term $V_{dip} = -E_{ext}\frac{r_0^2}{r}\sin\theta$ that can be written as $V_{dip} = V_{0\,Dip}\frac{r_0}{r}\sin\theta$, with $V_{0\,Dip} = -E_{ext}\, r_0$. In terms of complex potential, this classical model of the dipole is described by

$$V_{dipA} = \mathrm{Re}\left(jV_{0\,Dip}\frac{r_0}{z}\right). \qquad (11)$$

With this expression of the distribution created by the dipole, it becomes possible to eliminate the artefact of the variation of the potential on the wire. This artefact is due to the use of equation (7) that does not describe the wire geometry perfectly (it should be cylinder, not line). To check the validity of this model's dipole referred to as Model A, or *dipA*, the difference between $(V_{line} - V_{dipA})$ and V obtained by FEM is plotted in figure 5.

Compared to figure 4, figure 5 illustrates the improvement of the analytical expression but an error of 2×10^{-4} V still remains. It is also noticed that the error on the wire features a $V_{0Quad}\cos 2\theta$ variation, in agreement with our findings.

4.5. Improved dipole modelling

In spite of the good results found in the previous section, a discrepancy can be noted in figure 5 at large distances from the wire. In order to improve the modelling, the technique presented in [8] is adopted. First, the expression of the complex potential of a line distribution (with distributed charge λ placed at z_0) is recalled:

$$\Phi_l = \frac{-\lambda}{2\pi\varepsilon_0}\log(z - z_0). \tag{12}$$

A line dipole constituted of two opposite distributions placed at $z_0 \pm jy_0$ is then represented by

$$\Phi_d = \frac{-\lambda}{2\pi\varepsilon_0}\log\frac{z - jy_0}{z + jy_0}. \tag{13}$$

For $|z| >> |y_0|$, the following approximation holds

$$\Phi_d \cong \frac{p_0}{2\pi\varepsilon_0}\frac{1}{z}, \tag{14}$$

where $p_0 = 2jy_0\lambda$ is purely imaginary as the dipole is on the *y*-axis.

It has been noted in [8] that the distribution Φ_d of the line dipole is proportional to $-\frac{d\Phi_l}{dz}$, a property also reported in [9]. Generalizing to our case, one first considers the line model of the grid described by expression (A1); then the line dipole of the grid is obtained through differentiation:

$$\Phi_{dip} = \frac{p_0}{2\pi\varepsilon_0}\frac{\pi}{a}\frac{\cos\xi}{\sin\xi}. \tag{15}$$

Adopting this expression, the approximation of the complex potential on the wire is

$$\Phi_{dip}(r_0 e^{j\theta}) \cong \frac{p_0}{2\pi\varepsilon_0}\frac{\pi}{a}\frac{1}{\xi} = \frac{2jy_0}{2\pi\varepsilon_0}\frac{1}{z}, \tag{16}$$

leading to

$$V_{dip} = V(r_0 e^{j\theta}) \cong \frac{y_0}{\pi\varepsilon_0}\frac{1}{r_0}\sin\theta. \tag{17}$$

Identifying equation (17) with equation (10) gives $\frac{y_0}{\pi\varepsilon_0 r_0} = V_{0Dip}$. Then expression (15) becomes $\Phi_{dip} = jV_{0Dip}\frac{\pi r_0}{a}\cot\xi$, and finally

$$V_{dipB} = V_{0Dip}\frac{\pi r_0}{a}\mathrm{Re}\left(j\cot\xi\right). \tag{18}$$

Equation (18) expresses the dipole contribution when the conducting cylinder is placed in the non-homogeneous external field created by the grid between the plates.

In order to check the validity of this model, the surface plot of the difference between V_{FEM} and $(V_{line} - V_{dipB})$ is given in figure 6.

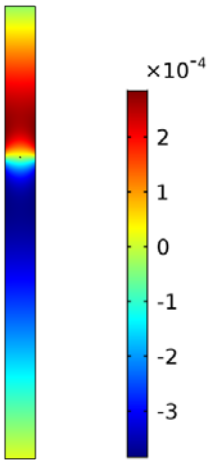

Figure 5. Model A of the dipole for an asymmetric case: surface plot of $V_{FEM} - (V_{line} - V_{dipA})$.

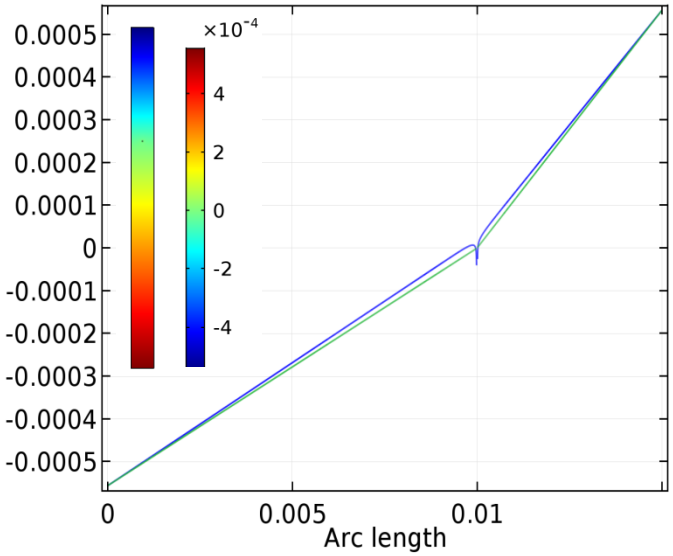

Figure 6. Model B of the dipole for an asymmetric case. $V_{FEM} - (V_{line} - V_{dipB})$ along the line $x = 0$. Inset: General view over the computational domain.

The comparison between figures 5 and 6 shows that both models A and B yield an error with same order of magnitude. However, the error of model B features a linear variation due to the fact that $\mathrm{Re}(j\cot\xi) \xrightarrow[|y|\to\infty]{} \pm 1$. Model B can then be improved by subtracting a linear term V_{dip_corr} of amplitude $V_{0Dip}\dfrac{\pi r_0}{a}$. The residual error is shown in figure 7.

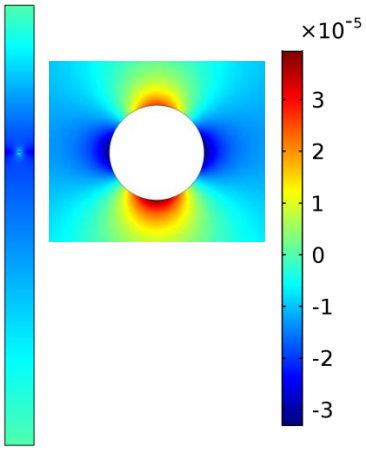

Figure 7. General and close view around the wire of $V_{FEM} - (V_{line} - V_{dipB} - V_{dip\_corr})$ for an asymmetric case

This new model has improved the theoretical determination that now leads to an error of 3×10^{-5} V.

5. Conclusion

The potential distribution around conductors of a grid has been studied from a well-known formula given by Erskine for MultiWire detectors. In the symmetric case where the grid is placed midway between two grounded plates, it has been shown that the error due to the almost but not exactly circular equipotential has a quadrupole-like contribution. This point has been checked through Finite Element Model analysis. After solving the electrostatic problem for the general geometry, it has been proved that a dipole contribution also exists in this case with a rather large amplitude. This dipole was then studied using a classical model and an advanced technique suitable for this geometry has been proposed. Finally this paper provides corrective terms of Erskine´s equation that yield at least a 10^{-6} accuracy, as reported in table 1.

Table 1. Order of magnitude of the relative error between FEM (with 10^{-9} error) and different models.

Symmetric	Equation (3)	10^{-6}
Symmetric with model of the quadrupole	Equations (3), (6)	10^{-8}
Asymmetric	Equation (7)	10^{-3}
Asymmetric with model A of the dipole	Equations (7), (11)	10^{-5}
Asymmetric with model B of the dipole	Equations (7), (18)	10^{-6}

Table 1 also shows that the error for the symmetric case is negligible, justifying why in the past, little attention was paid to the modelling issue. This does not apply to the general (asymmetric) case anymore.

6. Appendix

The general case where the grid is not centralized is somewhat more complicated than the symmetric one. Special functions can be invoked [1,3,7], but some of them are not embedded in Comsol Multiphysics®. Another method consists in assuming that the total potential is due to the one created by an isolated grid and superposing an external field [8]. This method gives good insights into the potential but it does not solve the electrostatic problem entirely, since the external electric field also depends on the potential. We can also find in [10] an expansion of the potential using separation of variables and eigenfunctions of the Laplace problem.

In their book [3], the authors present a technique based on the easy-to-obtain configuration of a grid above an infinite plane. As sketched in figure 2, the general case is decomposed into a grid (with linear charge λ) over a grounded plate, plus a two-plate capacitor with surface charge σ_P.

First is recalled the expression of complex potential for an isolated grid placed in the plane $y = 0$:

$$-\frac{\lambda}{2\pi\varepsilon_0}\log\left(2\sin\xi\right). \tag{A1}$$

For a grid placed above a grounded plate situated at $z_0 = -jL_1$, the application of image theory gives

$$-\frac{\lambda}{2\pi\varepsilon_0}\log\frac{\sin\xi}{\sin\left(\xi+\xi_0\right)}, \tag{A2}$$

with $\xi_0 = 2j\pi\frac{L_1}{a}$. The different approximations of expression (A2) are easy to derive and are indicated in [3].

Finally, adding to (A2) the constant offset V_1 and the linear expression of the potential for a two-plate capacitor, the superposition represented in figure 2 is expressed by equation (7).

The boundary conditions $V_{line}(0) = V_G - V_1$ and $V_{line}(z = jL_2) = V_2 - V_1$ are two equations depending on the unknowns λ and σ_P. This 2×2 system is written in a matrix form, using a convenient equivalent charge density of the grid $\sigma = \frac{\lambda}{a}$:

$$\begin{pmatrix} V_G - V_1 \\ V_2 - V_1 \end{pmatrix} = \frac{1}{\varepsilon_0} \begin{pmatrix} L_1\left(1 - \frac{a}{2\pi L_1}\log\rho\right) & L_1 \\ L_1 & L_1 + L_2 \end{pmatrix} \begin{pmatrix} \sigma \\ \sigma_P \end{pmatrix}. \quad \text{(A3)}$$

Inversion of this system gives the expression of the charges λ and σ_P as functions of V_G, V_1, and V_2:

$$\lambda = CV_0, \quad \text{(A4)}$$

$$\sigma_P = -\frac{L_1}{L_1 + L_2}\frac{C}{a}\left[V_G - V_1 + (V_2 - V_1)\left(1 - \frac{a}{2\pi L_1}\log\rho\right)\right], \quad \text{(A5)}$$

with $C = \frac{2\pi\varepsilon_0}{2\pi\frac{L_e}{a} - \log\rho}$, $V_0 = V_G - \frac{L_2V_1 + L_1V_2}{L_1 + L_2}$ and $L_e = \frac{L_1L_2}{L_1 + L_2}$.

It can be checked that, in the symmetric case, the surface charge on each plate is half the one distributed on the grid, *i.e.* $\sigma_P = -\frac{\lambda}{2a}$.

References

[1] Morse P M and Feshbach H 1953 *Methods of Theoretical Physics* McGraw Hill p 1241

[2] Sekar S and Stomberg H 1981 On the prediction of current-voltage characteristics for wireplate precipitators *J. Electrostat.* **10** 35-43

[3] Blum W and Rolandi L 1994 *Particle Detection With Drift Chambers* Springer-Verlag

[4] Erskine G A 1972 Electrostatic problems in multiwire proportional chambers *Nucl. Instr. And Meth.* **105** 565-72

[5] Read F H *et al*. 1999 Short and long-range penetration of fields and potentials through meshes, grids or gauzes, *Nucl. Instr. and Meth.* **427** 363-7

[6] Katagiri *et al*. 2010 Numerical analysis of the space charge effect in a MWPC *J. Plasma Fusion Res.* **9** 614-9

[7] Tomitani T 1972 Analysis of potential distribution in a gaseous counter of rectangular cross-section *Nucl. Instr. and Meth.* **100** 179-91

[8] Bunemann O *et al*. 1949 Design of Grid Ionization Chambers *Can. J. Res. A* **27** 191

[9] Durand E 1966 *Electrostatique, Tome II* Masson p 236

[10] McDonald K T 2003 Notes on Electrostatic Wire Grids http://hep.princeton.edu/~mcdonald/examples/grids.pdf